ThermoAcoustics and the Rijke Tube: Experiments, Identification, and Modeling

Jonathan Epperlein, Bassam Bamieh and Karl Åström

Introduction

The Rijke tube [1] is a classic experiment that is relatively simple and inexpensive to build in a typical university laboratory. Despite its construction simplicity, it can serve to illustrate a wide variety of mathematical modeling, empirical identification, verification and feedback control techniques. As such, it is suitable for use in both advanced undergraduate and graduate controls laboratory courses.

The Rijke tube also serves as prototypical experiment for research and study of *thermoacoustic phenomena* in which heat transfer and acoustics are dynamically coupled. This experiment is perhaps the simplest illustration of the phenomenon of thermoacoustic instabilities, which typically occur whenever heat is released into gas in underdamped acoustic cavities. The heat release can be due to combustion or solid/gas heat transfer. Under the right conditions, the coupling between the acoustic and heat release dynamics in the cavity becomes unstable. This instability manifests itself as a sustained limit cycle resulting in audible, powerful pressure oscillations. Thermoacoustic instability phenomena are most often encountered in combustors [2], [3], where the resulting powerful pressure waves are undesirable due to the danger of structural damage as well as performance degradations. In this context, they are often referred to as combustion instabilities, and are notoriously difficult to model due to the additional complexity of combustion dynamics [4], [5]. The advantage of the Rijke tube is that it generates thermoacoustic instabilities without a combustion process. The absence of combustion renders the mathematical modeling and subsequent system analysis problems significantly more tractable, yet many of the identification and feedback control issues involved in combustion instabilities are present in the Rijke tube. Thus, this experiment provides an easily accessible platform within which one can explore the myriad issues relevant to thermoacoustic instabilities and their control.

The present paper aims at introducing the Rijke tube as both an experimental and theoretical platform to explore thermoacoustic dynamics and their control. It consists of two complementary parts. The first is an experimental investigation of the dynamics of the Rijke tube using closed-loop identification and model validation. The second part details the derivation of a control-oriented model from the simplified thermoacoustic physics of one-dimensional gas dynamics. This model is examined using LTI system tools such as the root locus and the Nyquist criterion, giving insight into the open-loop instability and the effects of feedback control. The first part is an empirical approach that requires little knowledge of the underlying physics, and it is remarkable that one can obtain rather useful and predictive models of the system with this approach. In our courses, most students who have performed this experiment and subsequent analysis did not start out with any knowledge of thermoacoustic physics. Further insight is obtained by combining the results of the feedback control experiments with the theoretical models developed in the second part. The section on mathematical modeling has been made compact and self contained, as well as easily accessible to readers with a control engineering background. This perhaps distinguishes the present paper from other excellent treatments of the Rijke tube in the literature [6], [7], [8], in that the self-contained presentation is written for a control engineering audience.

Prior to embarking on the two main components of this paper, a brief description of how a typical Rijke tube experiment is conducted, the observations that can be made, and the construction of the apparatus are given.

Observations of the Rijke Tube and its Control

By way of an introduction, some basic observations that can be quickly made in the laboratory are described. These observations set the stage for the many modeling, identification and control questions that can be subsequently posed and investigated. Figure 1(a) illustrates the basic operation of the Rijke tube. A heating element (typically a resistive coil) is placed in the bottom third of a vertical open glass tube; for details on the specific setup here at UCSB, see "Construction of the Rijke Tube Apparatus." If the coil is sufficiently hot, a steady upwards flow of air is achieved. An increase in the power to the coil causes an increase in the air flow, and at some critical value of this power, the tube begins to emit a loud, steady "hum" like a pipe organ. A decrease in the power to the coil will cause the hum to die out. A measurement of the frequency of that sound, and assuming typical sound velocity in air at room temperature, shows the wavelength to be equal to twice the length of the tube. This is consistent with a half-wavelength standing wave in the tube.

The next step is to experiment with a simple active acoustic feedback scheme. A speaker is placed a slight distance under the tube. The speaker is powered by a variable gain
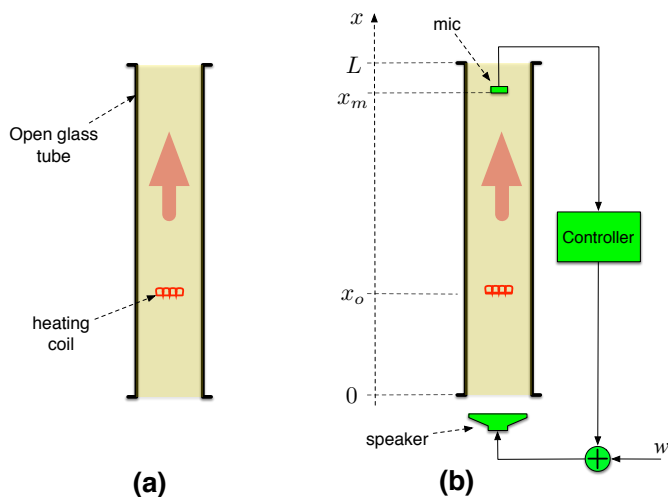
Figure 1. **(a)** The Rijke tube shown with a heating element placed towards the bottom (suspension mechanism for coil not shown). Upward arrow indicates steady air flow caused by the coil's heat. **(b)** The Rijke tube with microphone, speaker and feedback controller. The external signal w is used for closed-loop identification.

amplifier with input from a microphone that is placed near the top of the tube. This is illustrated in Figure 1(b), where the amplifier is referred to as the controller. This arrangement can be thought of as simple proportional feedback. If the power to the coil is made sufficiently high to cause the tube to hum, one can experiment with the feedback gain to investigate its effects. If the sign of the feedback gain is chosen correctly, it is observed that as the gain is increased upwards from zero, there is a critical value of the feedback gain which causes the loud hum to quickly disappear. A natural question is whether this represents a stabilization of an unstable process, or possibly some form of noise cancellation. A quick check of the control signal (speaker input) reveals that signal to be near zero, indicating that the speaker is indeed stabilizing the thermoacoustic instability rather than canceling the noise produced by it. This simple stabilization scheme allows for closed-loop system identification to be done, from which an empirically determined open-loop transfer function can be obtained.

After stabilization by simple proportional feedback, the next step is the investigation of the gain margin and what happens at high gains. It is observed that with further increase in the feedback gain, the tube begins to emit a loud "screech" sound, at a different and higher frequency than the hum observed earlier. A measurement of the screech frequency yields that it is roughly a harmonic of the originally observed hum frequency. Often it will be either the third or fifth harmonic with other harmonics occurring less often. Exactly which of the harmonics it is turns out to depend on the microphone position, and is an important feature of the problem which can be later used for the model validation component of the experiment. In summary, the instability at high feedback gains (the screech) occurs due to the right half plane zeros inherent in this system. The open-loop pole locations are determined by

the tube's acoustics and are largely independent of speaker and microphone position. However, the open-loop zero locations, which influence the high-gain instability, are dependent on actuator and sensor location.

Empirical Investigation of the Rijke Tube

The experimental exploration of the Rijke tube begins with establishing the conditions for the initial thermoacoustic instability as a function of heater power input. The effects of proportional acoustic feedback are then investigated through initial stabilization and then observing instabilities at high gains. Once a stable system is established, closed-loop identification is performed and a model from frequency response data is obtained. A root locus analysis of the identified model is used to explain the basic thermoacoustic instability. Locations of the open loop poles and zeros of the identified model play an important role in the dynamics, and root locus analysis is used to further validate the model using observations of the high-gain instabilities.

Observing the Thermoacoustic Instability

The initial operation of the Rijke tube is quite simple: The heater coil power supply is turned on and increased slowly. During this process one can feel the upward flow of hot air by placing the hand slightly over the tube top as depicted in Figure 1(a). There is a critical heater power beyond which the tube will begin to hum loudly. The increase in sound level up to saturation occurs in a couple of seconds. If the heater power is decreased and then increased again, a slight hysteresis phenomenon can be observed. The sound frequency f is easily measured with an oscilloscope (about 143 Hz in our setup), and using the speed of sound under standard conditions $c = 343$ m/s, its wavelength

$$\lambda = c/f$$

is approximately equal to twice that of the tube. This is consistent with a half-wavelength standing wave in the tube, which is the fundamental mode of a tube open at both ends. The basic physics of that mode are illustrated in Figure 3.

Proportional Acoustic Fedback

When microphone, DAQ board and speaker are connected in the arrangement shown in Figures 1(b) and S1, proportional feedback can be applied to the Rijke tube. It is observed that as the gain of the power amplifier is increased, there is a critical gain value $K_{\min}$ above which the tube's hum will quickly disappear. This is usually an impressive demonstration of the power of feedback.

Since many students who perform this experiment are not familiar with acoustics, they are often unsure as to what
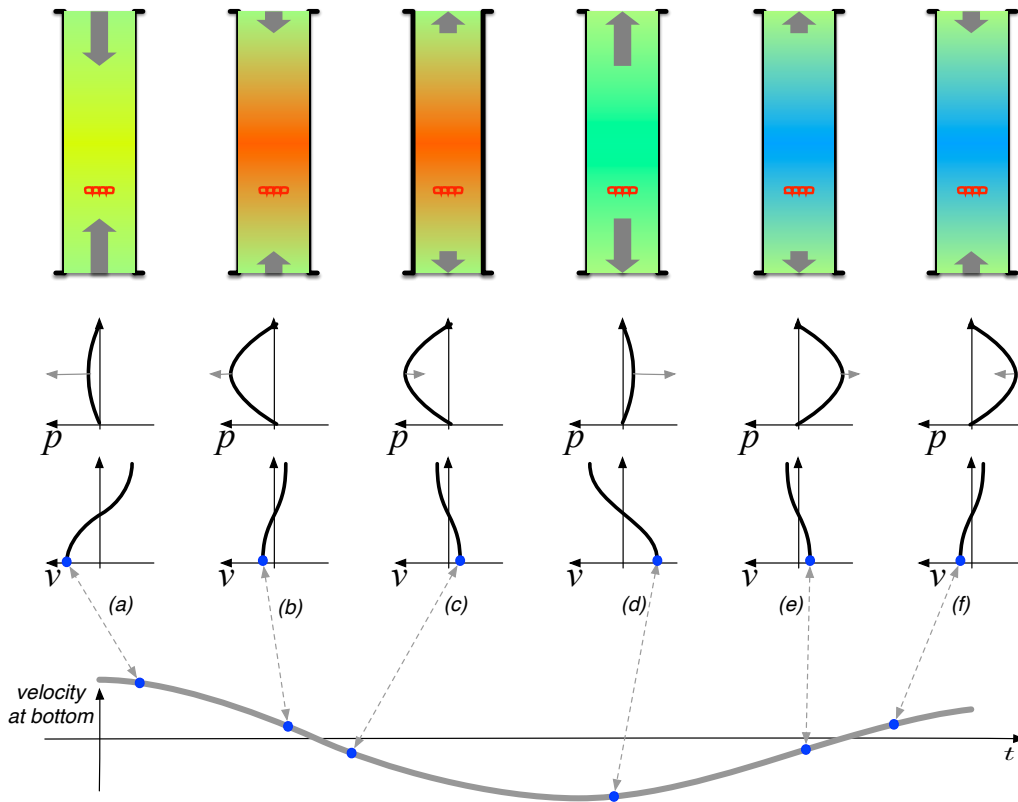
Figure 3. A diagram of the fundamental acoustic mode of the Rijke tube showing its "half-wave" nature. In the top three rows, the spatial waveforms are shown. Acoustic pressure is shown in color and the acoustic velocity at the ends is illustrated as arrows. The bottom row depicts one period of the temporal waveform of the velocity at the bottom of the tube. In phase *(a)*, the pressure just started increasing in the center of the tube due to the air rushing in, which in *(b)* has led to the pressure achieving a maximum at the center, while simultaneously the velocity has been decreased by the resulting pressure gradient. In *(c)*, the pressure gradient has inverted the velocity, so that air now starts rushing out of the tube with *(d)* increasing velocity, until *(e)* the pressure reaches a minimum in the center and the gradient leads to *(f)* air being sucked in again, until *(a)* pressure moves towards its maximum again and the cycle repeats.

is happening when the tube's hum disappears. They often say that the tube's noise has been "cancelled," probably because of familiarity with noise-canceling headsets. However, the process here is fundamentally different. The feedback has *stabilized* the thermoacoustic instability which caused the limit cycle in the first place. To verify the distinction between stabilization and noise cancellation, it suffices to observe the control signal into the speakers terminals on an oscilloscope as the critical feedback gain is reached and the hum disappears. The oscilloscope will show that the control signal decays rapidly and hovers around zero as the critical stabilizing feedback gain value is reached. In contrast, a noise-canceling system would have a persistent non-zero control signal canceling the persistent noise.

Interesting phenomena occur at higher gains. There is a critical higher gain value K_{max} above which a new instability is triggered. When that gain is reached, the tube will begin to "screech" loudly. A measurement of that screech frequency reveals it to be a harmonic of the initial fundamental hum frequency (as depicted in Figure 4). Exactly which harmonic it is will depend on the details of the experimental set up (in ours it is typically the 3rd or 5th harmonic). This phenomenon is however repeatable if the experimental setup — microphone,

speaker and heater locations — is unchanged. The screech frequency should be noted as it can be predicted from a root locus analysis of the identified system model, and therefore can be used to validate that model.

Closed-Loop Identification

In this empirical approach to the Rijke tube, no physical modeling is done. Instead, system identification tools are used to obtain information about the dynamics. The Rijke tube with the heater on is an unstable system, and therefore must be identified while operating in a stabilizing closed loop. A conceptual block diagram of the Rijke tube system is shown in Figure 5. The working assumption is that the the power and pre-amplifier, as well as the microphone and speaker can all be described by pure proportional gains. In reality, they are designed to pick up and transmit sounds audible to humans, hence their frequency responses outside the hearing range (20-20,000 Hz) will be quite poor and not flat; however, in the frequency range of interest in this experiment (typically 100-1,000 Hz) where the Rijke tube acoustic dynamics are dominant, experience has shown this working assumption to be reasonable. Therefore in the diagram of Figure 5 the speaker,
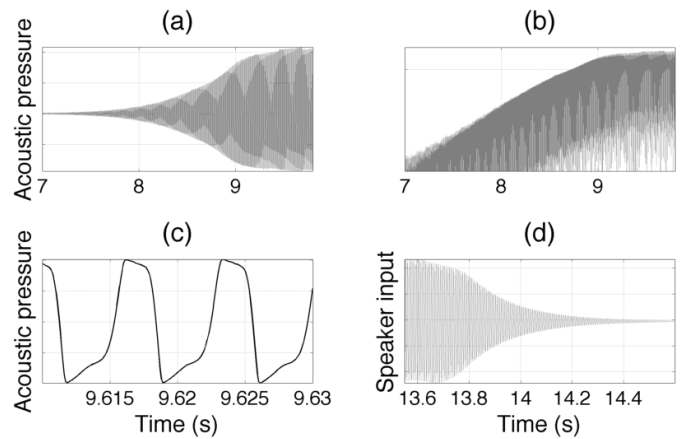
3

Figure 2.   Time trace of the microphone signal **(a)** at the onset of instability showing growth, and then saturation of the limit cycle. Linear growth on a semilog plot **(b)** of the signal's envelope confirms initial exponential growth of its amplitude. A zoomed-in picture **(c)** shows the periodic, but non-symmetric limit cycle behavior. With appropriate proportional feedback, the limit cycle is stabilized as this trace of the speaker's input signal **(d)** shows.
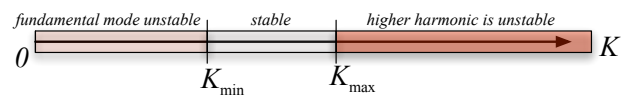
Figure 4.   A depiction of the effects of proportional feedback on the Rijke tube. A minimum feedback gain $K_{\min}$ is necessary to stabilize the unstable fundamental mode. There is then a critical higher gain $K_{\max}$ beyond which a higher harmonic mode of the tube becomes unstable yielding a high-pitched screech.

Rijke tube, mic and pre-amp blocks are lumped together and regarded as simply "the Rijke tube," and the variable gain power amp is regarded as a pure proportional gain. The "test signal" is generated in Simulink and added to the control signal, it provides the input for the closed loop system identification process.

Closed-Loop System Identification: Care needs to be taken when identifying systems in a closed loop, since simply recording the plant input and output and applying open-loop identification techniques, ignoring the fact that the input is the result of feedback, might yield wrong results; in particular the property of consistency, i.e. that collecting an infinite amount of data will result in an exact identification of the underlying system, is lost. The reason is that most
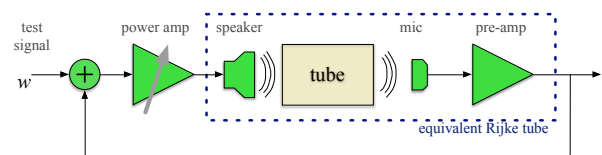
Figure 5.   Equivalent block diagram of the Rijke tube with acoustic feedback. The speaker, microphone and pre-amp transfer functions are assumed as unity and are lumped together with that of the Rijke tube. The power amplifier is simply regarded as a variable gain. The external test signal w is used for closed-loop identification.

identification techniques start from a system model of the form $y(t) = F(e^{j\omega})u(t) + \nu(t)$, where ν represents measurement noise, and it is assumed that noise and input are uncorrelated. However, if the system operates in closed loop, the input $u(t)$ is determined from the measured output, and hence now correlates with the measurement noise. The simplest workaround, and the one chosen here, is the so-called *indirect method*: As shown in the conceptual block diagram in Figure 5, an exogenous test signal w is added into the loop. The structure of the model then is again $y(t) = T(e^{j\omega})w(t) + \nu(t)$, but now $T(e^{j\omega})$ is the closed-loop transfer function, and w and ν are indeed uncorrelated. $T(e^{j\omega})$ can then be identified with any open-loop technique, and the open loop $F(e^{j\omega})$ can be recovered by simple algebra. For more background and more sophisticated methods see e.g. [9], [10]. Here, the closed-loop transfer function from the test signal w (added into the input of the power amplifier) to the microphone output y is

$$ T = \frac{KF}{1 - KF}, $$

where K is the aggregation of all the gains of the other components (assumed to be independent of frequency) in the loop. Once T is identified, F is obtained by inverting the above relation

$$ F = \frac{1}{K}\frac{T}{1 + T}. \tag{1} $$

It would be very difficult to obtain a value for K, which for instance incorporates the unknown conversion factor from pressure to voltage output by the microphone, but the above equation shows that the poles and zeros of F can be identified from those of T without knowing K. In other words, F is identified up to an unknown gain factor $\frac{1}{K}$.

Open-Loop Identification Method: The dynamics underlying the Rijke tube are a combination of acoustics and heat transfer, and are thus of relatively high order (in fact, they are infinite dimensional). Nonparametric frequency-domain identification schemes are better suited to those types of systems than time-domain based ones, since one is not forced to select a model order a priori. Instead, the frequency response $T(e^{j\omega})$ is identified directly, and then a least-squares based method is used to fit a model of appropriate order over the identified frequency range. So-called spectral methods (see e.g. [11, Ch. 6]) estimate the frequency response as the ratio of the cross spectrum $\Phi_{yw}(\omega)$ of output and test signal, and the spectrum $\Phi_w(\omega)$ of the test signal. The MATLAB System Identification Toolbox [12] offers two implementations of these methods, spa and spafdr. While both estimate the cross spectrum and input spectrum by applying a smoothing window to what roughly amounts to the discrete Fourier transforms of input and output data, spa performs the windowing in the time domain, whereas spafdr applies the window in the frequency domain. The expected sharp peaks in the frequency response require fine resolution in frequency; since a narrow frequency-domain window, which is what is required, corresponds to a wide time-domain window, using spafdr allows one to specify a small (frequency-domain) window, resulting in a drastic decrease in computation time compared to the large
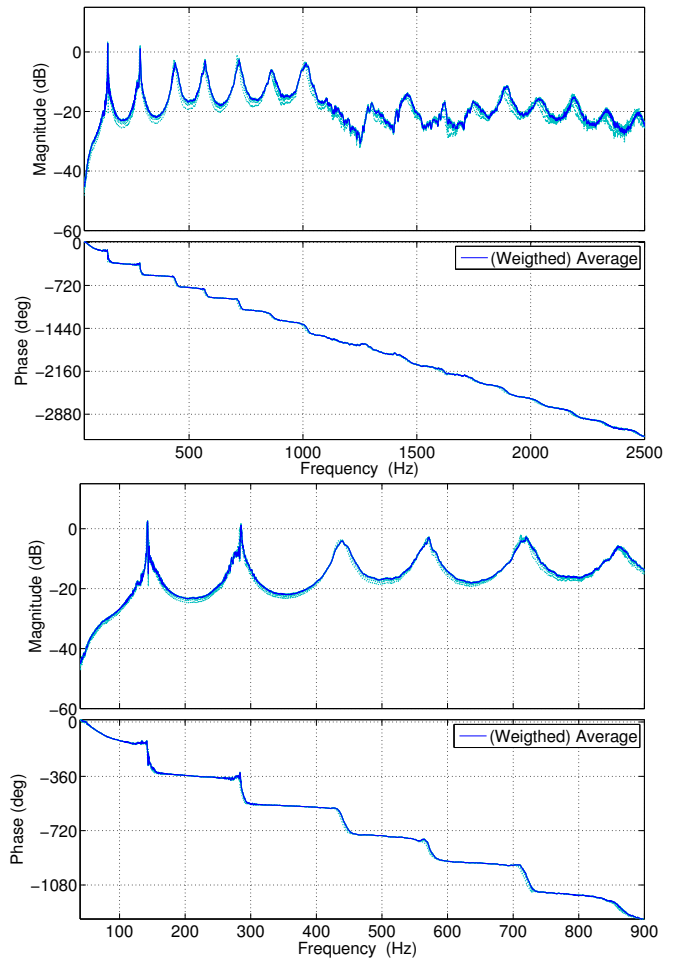

Figure 6.   Closed-loop frequency response obtained with a sine sweep over the range of 0-2.5 kHz (top) and 0-900 Hz (bottom). The response below 20Hz, which is outside the audible range, and above 1kHz is likely dominated by microphone and speaker distortions. The range 0-1 kHz however exhibits typical wave-like dynamics with resonances occurring at multiples of the fundamental frequency. Note that here and in all Bode plots that follow, a linear frequency axis is used to emphasize the pattern of a fundamental frequency with harmonics.

(time-domain) window that would have to be specified to achieve the same resolution using spa. (Another important distinction between spa and spafdr is that the latter allows for frequency dependent resolution (hence the name), but we did not make use of this feature.) The least-squares fit is then performed using the function clsfits from the FREQID Toolbox for MATLAB [13], [14].

Test Signal: A test signal should have rich frequency content, while, due to actuator and sensor limitations in physical systems, amplitudes should be kept reasonably small. Popular choices include white noise, Schroeder-phased sinusoids [15] and sine sweeps (also known as chirp signals). We experimented with all three types of signals, and sine sweeps, which have been found to be beneficial in the identification of acoustic systems [16], emerged as the most effective choice; all shown data was collected using a sweep over the shown frequency range.

For the identification experiment, the tube is first brought to a hum. Then, the feedback with a stabilizing gain is turned on, and the test signal is added to the feedback signal, as shown in Figure 5. The microphone signal is recorded for the duration of the experiment (in our case about 120 s), and together with the applied test signal forms an input-output pair, which is all the data needed to obtain a spectral estimate. To minimize the effects of random noise, this is done several times, and an average of the estimated frequency responses is formed. Figure 6 shows an averaged closed-loop frequency response along with the individual experiments. This response with several very lightly damped modes at integer multiples of a fundamental frequency has the signature of wave-like dynamics. The fundamental frequency corresponds very closely to the frequency of the hum observed in the non-stabilized Rijke tube.

In order to perform the least-squares fit of a finite dimensional transfer function model for T to the estimated frequency response, a value for the model order needs to be selected. Figure 7 shows a 12$^{\text{th}}$ order transfer function fit, which nicely captures the first 6 harmonics in the frequency response.

To obtain the transfer function F, a parametric model of the open loop, the fitted model T is then plugged into (1). Of course it is also possible to apply (1) to the nonparametric estimated frequency response at each frequency, thereby obtaining a nonparametric model of the open loop. Both of those possibilities are compared in Figure 8, they are in close agreement, which is encouraging. Note that, while the phase at the first peak of the closed loop T drops by 180$^\text{o}$ indicating a stable pole slightly to the left of the imaginary axis, it increases by 180$^\text{o}$ in the open-loop response, indicating a pole slightly in the right half plane (RHP).
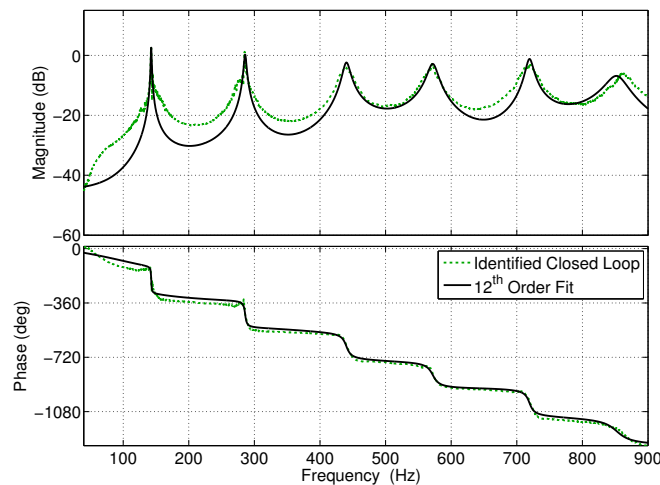

Figure 7.   Closed-loop frequency response obtained by a non-parametric spectral estimation, and a 12$^{\text{th}}$ order least-squares fit. Note that due to the log-scale, the seemingly large deviations in the ranges between the peaks are actually very small.
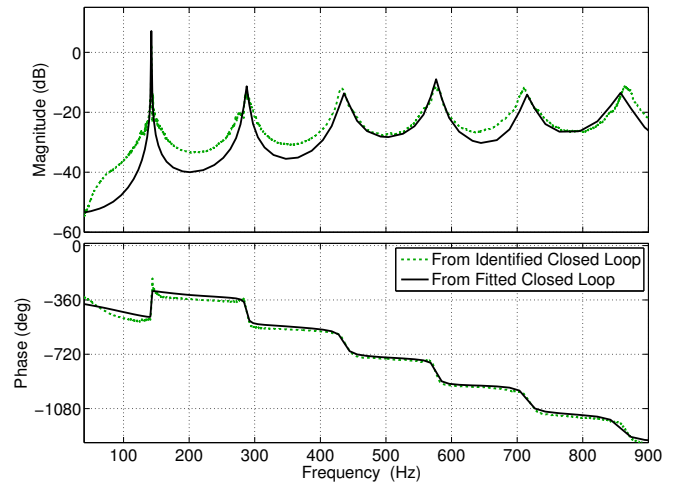

Figure 8.   Open-loop frequency responses, obtained by applying (1) to the identified closed-loop response at every frequency (green) or to the fitted closed-loop response (black).

Model Validation: Root Locus Analysis

The model F of the open loop obtained in the last section can now be used to explain the experimental observations. The root locus explains, why proportional feedback initially stabilizes the thermoacoustic instability, and why a higher frequency mode becomes unstable at high gains. It will also give a quantitative prediction of that higher frequency — a prediction that can be used to validate the model.
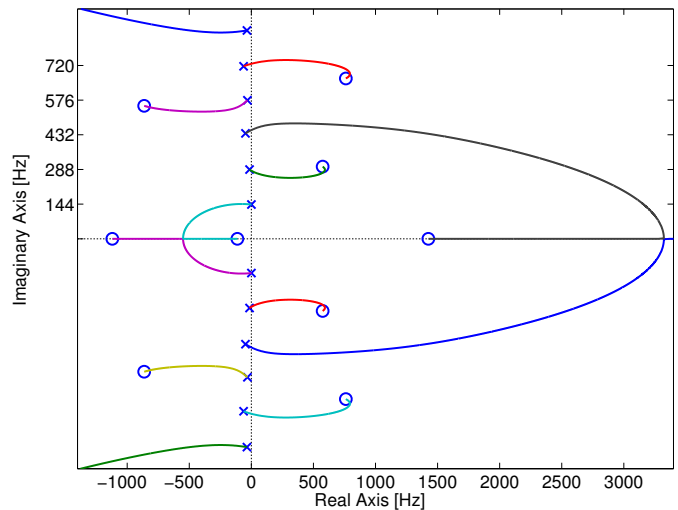
Figure 9.   A full view of the root locus of the identified open-loop model with variable proportional feedback control gain. The open-loop poles show the (unstable) fundamental mode at 144Hz and its (stable) harmonics very close to the imaginary axis. Several RHP open-loop zeros attract closed-loop poles into the RHP at high feedback control gains.

Figures 9 and 10 show the root locus of the identified open-loop dynamics. The pole pattern resembles that of a
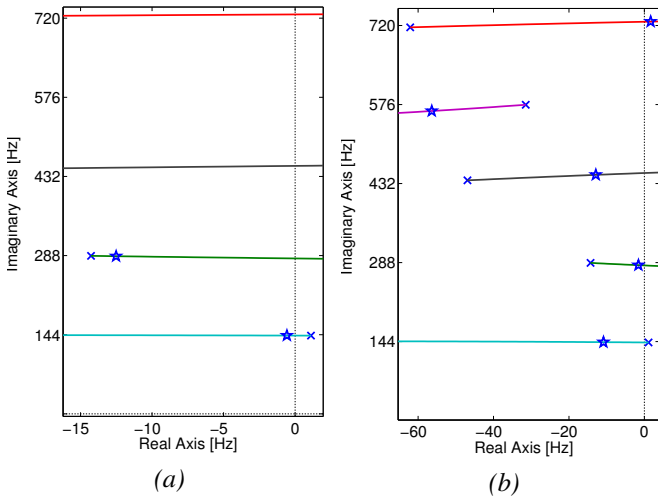
6

Figure 10. Root loci of the identified open-loop model F showing closed-loop pole locations (★) at gains that *(a)* just stabilize the unstable fundamental mode and that *(b)* make the fifth mode unstable.

damped wave equation, with imaginary parts of the poles being integer multiples of a fundamental frequency, and the real parts having successively higher damping as the mode frequency increases. As promised, the fundamental mode is unstable, having positive real part. The imaginary part of the fundamental mode corresponds to the hum frequency heard when the tube is initially powered on.

This system also has multiple RHP zeros which ultimately attract a subset of the initially stable open-loop poles into the RHP, thus causing instability to reoccur at high gains. Figure 10(a) shows the locus and the pole locations at the value of the gain sufficient to initially stabilize the fundamental mode (denoted $K_{\min}$ in Figure 4), all poles are in the left half plane. However, due to the presence of RHP zeros, some poles will eventually cross into the RHP as the gain is increased. Figure 10(b) indicates that for this particular identified model, it is the fifth harmonic mode that becomes unstable at higher gain (denoted $K_{\max}$ in Figure 4). The frequency of this mode must correspond to the frequency of the screech heard in the experiment as the system becomes unstable again at high feedback gains, which is indeed what we observed on the setup used to collect the identification data. This serves as a useful method of model validation.

Common Problems in the Identification Process

Often, the phase of the open-loop frequency response will also drop, instead of increase, by $180º$ at the first peak, i.e. the open loop is identified as stable, while we know that the open loop must be unstable. The stability of the open loop is very sensitive to the amplitude and phase of T at the first peak. This is most easily explained with an argument based on the Nyquist criterion: From (1), it is seen that F has the same poles as T in negative unity feedback, so stability of F can be assessed through the Nyquist criterion. In order for T

to encircle the critical point $(-1, 0j)$, one needs $|T| > 1$ and $\angle T = -180º$ at the same frequency. Inspecting Figure 6 again, one sees that for the presented data, the first peak reaches only about 2 dB, and the range for which it exceeds 0 dB is only about 1 Hz wide. Hence, if the peak is "cut off," the identification will result in a stable open loop. Likely culprits are insufficient frequency resolution and too much smoothing during the spectral estimation. This situation is detailed in Figure 11. If increasing the resolution and decreasing the smoothing do not help, a different speaker might be the solution; we found speakers to have quite different frequency responses, some added considerable phase lag.

It also might happen that the root locus predicts the higher harmonic instability incorrectly. This again indicates that the initial closed-loop identification step was inaccurately performed (insufficient or noisy frequency response data, order selected for the model fit too low, etc.). A repeat of the identification step with more care will typically resolve this issue and the more carefully identified model will then yield the correct prediction of the high gain instability.

Lastly, if experiments are run for a long time, the tube walls, especially around the heater, absorb a lot of heat. If the identification is stopped and restarted for a new run, there might be no initial humming, due to the tube walls heating the air around the heater to the point where the heat transfer between air and heater is insufficient to support the humming. In that case, one can only wait for the tube to cool off, or, if the setup admits, increase the power to the heater to increase the coil temperature.

Microphone position

The microphone position generically influences only the location of the zeros, not the poles, which is why its exact position was never stated. However, there are special locations that do yield interesting results. Figure 12 shows the identified open loops if the microphone is placed at three quarters, and at half the length of the tube. Doing so appears to "remove peaks," in the former case it would be every fourth, and in the latter case every even-numbered one.

This is relatively easily explained with the physical model of the transfer function developed in the modeling section, but there is also a very intuitive explanation: each peak corresponds to a mode, a standing pressure wave, in the tube; the standing wave corresponding to the first peak is a half-wave, for the second peak a full wave, and so on. Placing the microphone at e.g. the center means placing it where all the even numbered modes have a pressure node, and hence their contribution is not registered by the microphone, a pressure sensor.

This would not be surprising at all for a tube without a heater; that it still holds true with the heater indicates that its effect, the thermoacoustic effect, is pulling the first mode
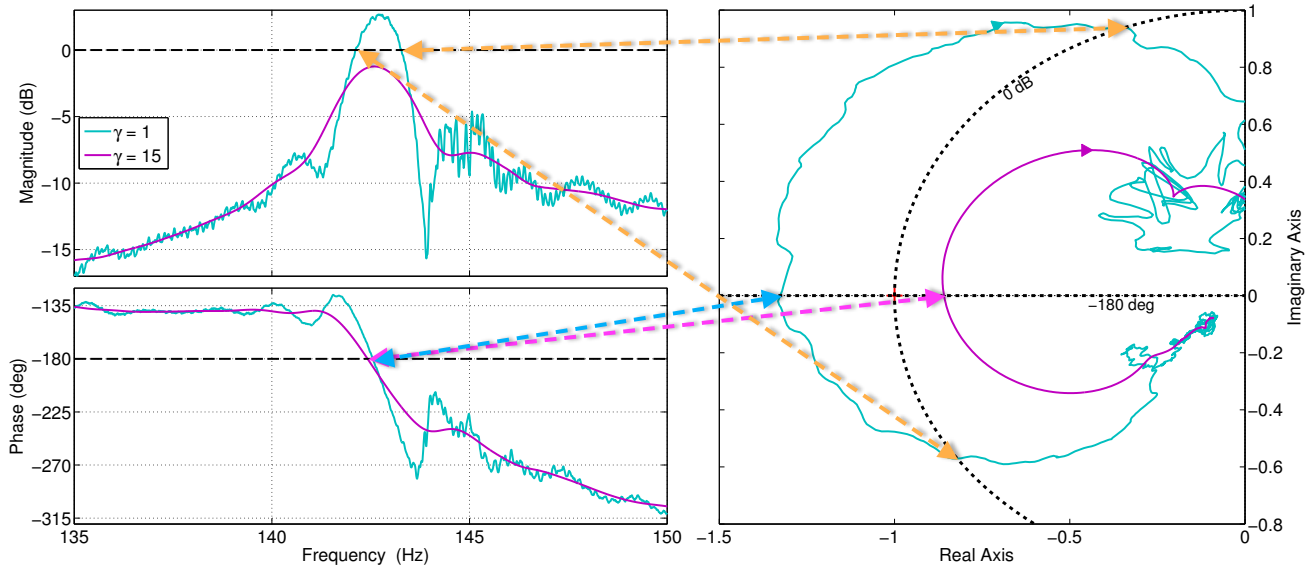
Figure 11. By comparing two frequency responses obtained from the *same data* with *different amounts of smoothing* (γ is passed to `spafdr` and corresponds roughly to the size of the smallest detail [12]), the difficulty in identifying an unstable open loop can be illustrated. The cyan and magenta frequency responses shown on the left appear to be qualitatively the same, thus one might tend to choose the magenta one as it looks smoother while still capturing the resonant peak. However, the most important feature – the corresponding unstable open loop – is not captured by this smoother response; this is immediately clear when considering the Nyquist plots, shown on the right: the magenta curve cannot loop around the critical point because it never leaves the unit circle. Note that even $\gamma = 15$ still corresponds to relatively little smoothing.

into the right half plane, but besides that, regular acoustics dominate the response.
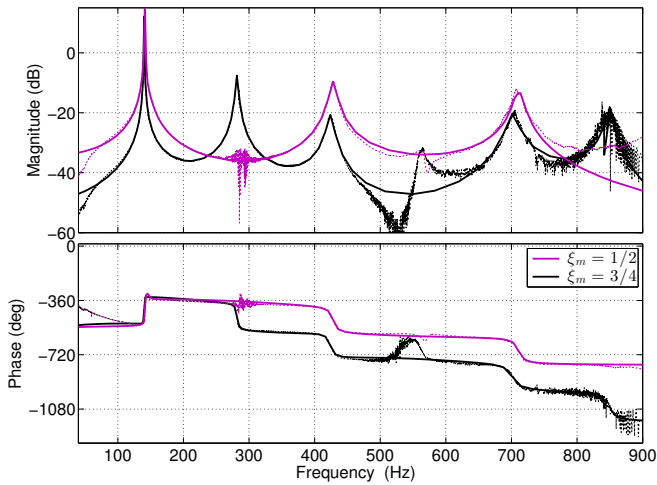

Figure 12. Bode plots for identified and fitted open-loop responses with different microphone positions. Placing the microphone in the middle of the tube ($\xi_m = 1/2$) seems to remove every other peak, while placing it at a quarter length from the tube attenuates the fourth peak only. The very ugly identification data at the removed peaks, and especially at the peak around 560 Hz, can be explained by the fact that perfect cancellation of a pole by a zero is virtually impossible; instead, one gets a pole and a zero very close together – notoriously difficult to identify.
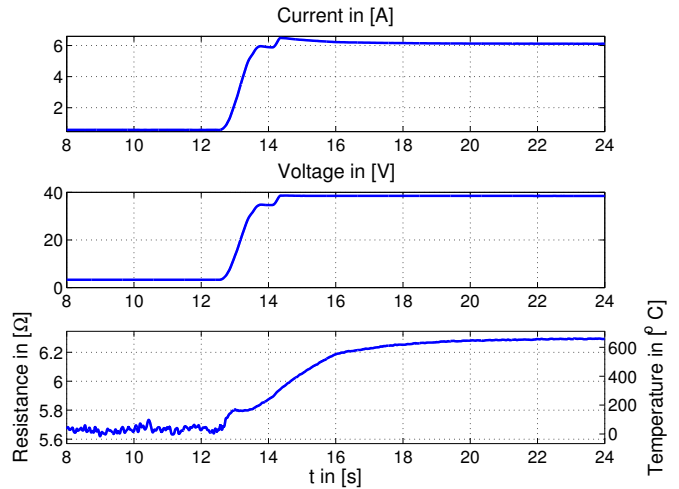
Figure 13. Smoothed time traces of voltage and current across the heating coil as the power is first set to a small value, and then increased until the humming sets in. The lower plot shows estimated resistance and temperature of the wire.

Estimating the wire temperature

Having an estimate of the temperature of the heating coil is of interest in and of itself, but it is also useful regarding the choice of materials to be used. It is straightforward to obtain a rough estimate from measurements of just voltage supplied to and current drawn by the heating coil by using the temperature dependence of the electrical resistance of the wire. The resistance R of a wire is commonly assumed to

depend on its temperature T affinely:

$$R(T) = R_0\big(1 + \alpha(T - T_0)\big),$$

where R_0 is the resistance at T_0, a known point of reference, and α denotes the (linear) temperature coefficient, which is tabulated for different materials. Typically, $\alpha > 0$, i.e. the resistance increases as the material heats up; for the Nichrome wire we are using, $\alpha \approx 1.76 \; 10^{-4}$ 1/K. The relationship can be inverted to

$$T = T_0 + \frac{R - R_0}{\alpha R_0}.$$

For the reference point (R_0, T_0), room temperature $T_0 = 293$ K is assumed. The resistance R_0 at room temperature is estimated by setting the power supply to a small voltage and recording current and voltage across the coil; then the supplied power is increased until the instability sets in and current and voltage are again recorded. Since current measurements are very noisy, in particular at low voltages, where the signal-to-noise ratio is smaller, averages over relatively long times are taken. An example time trace is shown in Figure 13, and one arrives at an estimate of

$$T_{\text{coil}} \approx 660^{\text{o}}\text{C} = 933 \text{ K}. \tag{2}$$

It is worth pointing out that while resistive thermometers are based on the same principle, the wire temperature here can by no means be used as a measurement of the gas temperature. For that to be the case, the thermal inertia of the wire would need to be several orders of magnitude smaller, which is why resistive thermometers use extremely thin wires and different materials.

Physical Modeling of the Rijke Tube

The remainder of this paper is devoted to physical and mathematical modeling of the Rijke tube at several levels of fidelity. The objective is to develop the most parsimonious model from a systems and controls perspective that can explain experimental observations of thermoacoustic instabilities, as well as the identification and feedback stabilization results. The key is to model the acoustic dynamics of the tube cavity, which are LTI, and the heat release at the coil, which contain a memoryless nonlinearity, separately. The feedback between those two physical phenomena is responsible for the thermoacoustic instability. As in the experimental section, it will be seen that LTI systems tools can explain much of the above phenomena.

A summary of the modeling results and their predictions about the instability is given next. This summary section can be largely read on its own; it assumes certain models for acoustics and heat transfer which are interpreted and motivated physically. Detailed derivations are postponed to subsequent sections for those readers interested in delving deeper.
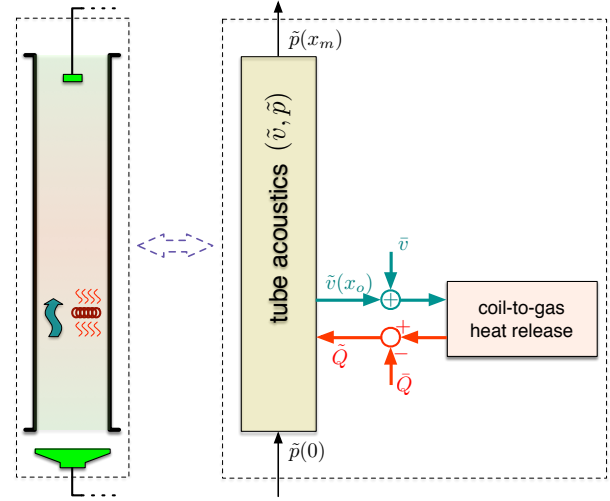

Figure 14. A block diagram depiction of the internal and the input-output dynamics of the Rijke tube. The "tube acoustics" block models the spatially distributed velocity $\widetilde{v}$ and pressure $\widetilde{p}$ fluctuations. Speaker and microphone signals are ideally modeled as pressure fluctuations $\widetilde{p}$ at the bottom end ($x = 0$) and mic position ($x = x_m$) respectively. The fluctuations $\widetilde{Q}$ of heat released from coil to gas act as a source term in acoustic dynamics as depicted by the horizontal arrows in diagram. In turn, this convective heat transfer process is influenced by the absolute gas velocity $\overline{v} + \widetilde{v}(x_o)$ near the coil. This internal feedback coupling between acoustics and heat release dynamics is the cause of the thermoacoustic instability.

Summary of Modeling and Analysis Results

A control-oriented model and physical description of the basic thermoacoustic dynamics can be summarized using two descriptive diagrams. Begin with Figure 14 where "tube acoustics" represents the dynamics of the velocity and pressure fluctuations $\widetilde{v}$ and $\widetilde{p}$. These are the fluctuations of the actual flow velocity v and pressure p about the nominal values $\overline{v}$ (the steady upward velocity) and $\overline{p}$ (atmospheric pressure) respectively. These fluctuations are also referred to as "acoustic velocity" and "acoustic pressure." Both velocity and pressure fluctuations are fields that vary along the length of the tube, while the nominal $\overline{v}$ and $\overline{p}$ are assumed to be constant in both time and space. As demonstrated later, the dynamics of $(\widetilde{v}, \widetilde{p})$ are described by a one-dimensional wave equation with the speaker (actuator) input modeled as a pressure boundary condition, while the microphone signal is the value of the pressure field at the microphone location. These acoustic dynamics constitute a linear time-invariant (though infinite-dimensional) system.

The second ingredient is to model the interaction between the heater coil and the surrounding air. In a steady situation with constant upward flow, heat is transferred from the heater to the upward-flowing gas conductively as well as convectively. The *convective* heat transfer is a function of flow velocity: the higher the velocity the more heat is transferred from the coil to the gas. If flow velocity near the heater is fluctuating (in time), then the amount of heat
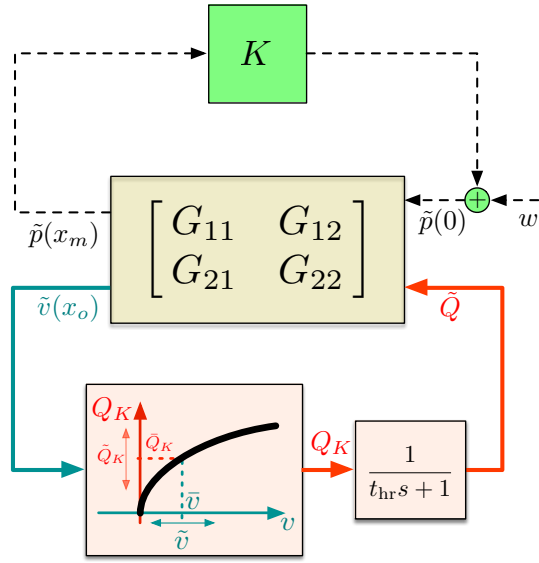
Figure 15. The nature of the feedback between acoustics and heat release depicted in Figure 14. The linear time-invariant (LTI) acoustic dynamics G transfer functions has lightly damped modes, which are in feedback with a first-order lag and a memoryless square-root type nonlinearity characterizing convective heat release. As a mapping from $\widetilde{v}$ to $\widetilde{q}$, the nonlinearity can appear as either high or low feedback gain at small or large amplitudes of $\widetilde{v}$ respectively. At small $\widetilde{v}$ amplitudes the lightly damped modes of the acoustics are destabilized by the high "effective gain" of heat release. As amplitudes of $\widetilde{v}$ increase, the effective feedback gain decreases so that conditions for a stable limit cycle are achieved.

transferred from coil to gas also fluctuates in response. This is shown in Figure 14 as a green wavy arrow depicting velocity fluctuations, and red waves depicting fluctuations of heat released from the coil. The block labeled "coil-to-gas heat release" represents the effect of local velocity fluctuations $\widetilde{v}(t, x_o)$ on fluctuations $\widetilde{Q}(t)$ in the amount of heat released. Vice versa, as will be demonstrated later, $\widetilde{Q}(t)$ acts as a source term in the gas dynamics (10), and can therefore be considered as an input to the acoustic part of the model. Within the "tube acoustics" block there is an acoustic feedback path from $\widetilde{Q}(t)$ back to $\widetilde{v}(t, x_o)$, which as explained earlier drives $\widetilde{Q}(t)$ through the heat release mechanism.

Figure 15 describes this feedback mechanism in a little more detail. The center block G is the LTI 2×2 transfer function matrix of the acoustics from the inputs to the outputs depicted in Figure 14. This matrix is made up of transcendental transfer functions since the underlying dynamics are infinite dimensional. For example, with undamped acoustics, coil location $x_o = L/4$, and microphone position $x_m > L/4$ it is

$$G(s) = \begin{bmatrix} \dfrac{\sinh\left(\frac{(L-x_m)}{c}s\right)}{\sinh\left(\frac{L}{c}s\right)} & \dfrac{\bar{\gamma}}{c}\dfrac{\sinh\left(\frac{L}{4c}s\right)\sinh\left(\frac{(L-x_m)}{c}s\right)}{\sinh\left(\frac{L}{c}s\right)} \\ \dfrac{1}{\bar{\rho}c}\dfrac{\cosh\left(\frac{3L}{4c}s\right)}{\sinh\left(\frac{L}{c}s\right)} & -\dfrac{\bar{\gamma}}{4\bar{\rho}c^2}\dfrac{1}{\cosh\left(\frac{L}{2c}s\right)} \end{bmatrix}, \quad (3)$$

for values and explanations of the involved parameters see Table II. The transfer function $G_{22}(s)$ is important for understanding the thermoacoustic instability since it is in feedback

with the heat release dynamics. Note that on the imaginary axis

$$\cosh\left(\frac{L}{2c}j\omega\right) = \cos\left(\frac{L}{2c}\omega\right),$$

and therefore G_{22} has infinitely many poles on the imaginary axis at

$$\omega_k = (2n-1)\frac{c\pi}{L}, \qquad n \in \mathbb{Z},$$

that correspond to the odd acoustic modes of a tube with two open ends, i.e. standing waves with wavelengths of $2L$, $2L/3$, $2L/5$ and so on. The fundamental mode corresponds to $n = 1$ and is the one depicted in Figure 3. If damping and/or radiative effects were to be included, those poles would be shifted to the left in a similar manner to those in Figure 9; this issue is further elaborated in "Wave Dynamics with Diffusion and Damping" on Page 19. The important fact to keep in mind is that G_{22} has *many very lightly damped poles* arranged at integer multiples of a fundamental frequency.

The heat release dynamics in the bottom blocks of Figure 15 combine two effects. The simpler one being a first-order lag with time constant t_{hr} representing the "thermal inertia" of the boundary layer surrounding the coil. The second effect is the square-root dependence of heat release on velocity. This is known as King's law [17], and it reflects that convective heat transfer is enhanced by increasing velocity, but the "enhancement rate" decreases as velocity increases. This effect of diminishing returns of heat release is responsible for the fact that an instability in the feedback loop between G_{22} and heat release ultimately produces a stable limit cycle. This is similar to what occurs in linearly unstable loops containing a saturation-type memoryless nonlinearity. The exponentially growing response due to the instability ultimately saturates, producing a stable limit cycle.

Hence, the heat release dynamics constitute a feedback from acoustic velocity to heat transfer. It is very important to distinguish this feedback from the stabilizing proportional feedback of the preceding section: On the one hand, the heat release process can be *interpreted* as an *internal* feedback loop, it connects two signals not accessible to measurement or direct manipulation; on the other hand, the stabilizing feedback is an *external* controller. In other words: the *open* loop identified in the previous section corresponds to the transfer function from $\widetilde{p}(0)$ to $\widetilde{p}(x_m)$ in Figure 15, which includes the *closed* loop of G_{22} and heat release. The above qualitative arguments hint that the key to quantitative understanding of the thermoacoustic instability is analyzing the linearization of this internal feedback loop, consisting of G_{22}, the first-order lag, and the linearization of the heat release square-root law, which can be modeled as a variable linear gain. It turns out that a root locus analysis accurately describes the effect of this gain as is demonstrated next.

The open-loop transfer function of the linearization of the lower feedback loop in Figure 15 is

$$-\frac{\bar{\gamma}}{4\bar{\rho}c^2}\frac{1}{\cosh\left(\frac{L}{2c}s\right)}\frac{1}{t_{\mathrm{hr}}s+1}f'(\bar{v}),$$
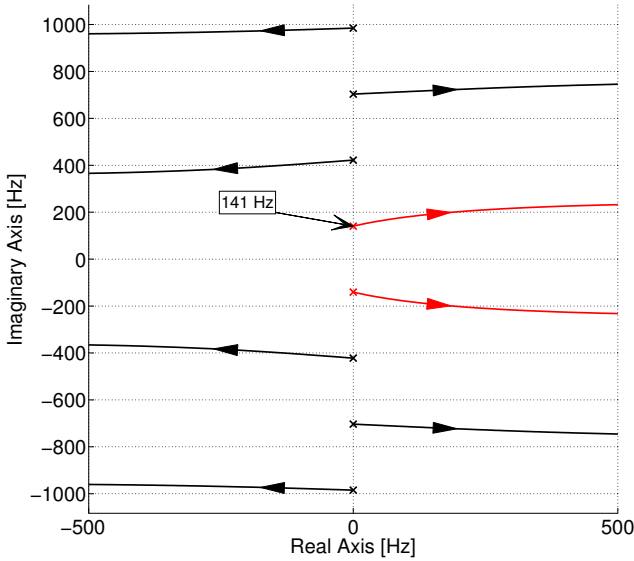
Figure 16. Root locus for the feedback interconnection of $G_{22}(s)$ and the linearized heat release dynamics in Figure 15. The plot should be interpreted as if it were shifted slightly to the left, as would be the case if realistic damping effects were included. The branch shown in red corresponds to the thermoacoustic instability; assuming standard conditions on air, its crossover point is at 141 Hz, very close to the frequency of the observed hum and the 144 Hz predicted by the identified model, see Figure 10. See Table II for the parameter values used.

where $f'(\overline{v})$ is the derivative of the square-root nonlinear gain at the steady upward flow velocity $\overline{v}$. This represents a linear positive feedback gain which depends on the operating condition $\overline{v}$. Thus the stability of the linearized closed-loop system can be completely characterized using the (negative gain) root locus of the transfer function

$$L(s) \;=\; \frac{1}{\cosh\!\left(\frac{L}{2c}s\right)} \frac{1}{t_{\mathrm{hr}}s + 1}. \qquad (4)$$

Since this transfer function has infinitely many poles, a little care is needed in generating the root locus. Figure 16 shows the locus of the zeros of $1 + k\,L(s)$ using a continuation (Newton) method in the positive real parameter k. The open-loop poles are the acoustic ones lying on the imaginary axis together with one pole on the negative real axis corresponding to the first-order lag in heat release dynamics. In reality, the acoustics have some damping and its corresponding poles lie slightly to the left of the imaginary axis as for example in Figure 9. Therefore the open-loop dynamics are stable, but have an array of very lightly damped poles. With the positive feedback from coil heat release, we see that half of the acoustic poles eventually move into the right half plane. The first pole (pair) to cross into the RHP corresponds to the fundamental frequency and is depicted by the red branches in Figure 16. Its imaginary axis crossing frequency of 141 Hz corresponds almost exactly to the frequency of the hum recorded at the onset of thermoacoustic instability. Once this instability is triggered, the system exhibits growing oscillations and leaves the linear regime (remember, the $\widetilde{\bullet}$ variables need to be small). Intuitively, the square root term then offers diminishing returns, i.e. at higher acoustic velocities, it almost saturates,

and even larger oscillations in velocity are not supported by the enhanced heat transfer anymore. The system is brought into a limit cycle, the shape of which can be seen in Figure 2(c).

Acoustic Dynamics from Mass, Momentum and Energy Balances

The basic features of the Rijke tube experiment can be captured using a simplified model of one-dimensional compressible gas dynamics. A brief description and derivation of the Euler equations of gas dynamics in one dimension is included in "One-dimensional Compressible Gas Dynamics" on Page 12. These are partial differential equations (PDEs) that describe conservation of mass, momentum, and energy, respectively. They can be written in several forms, and the form chosen here is the one that relates the time-varying density $\rho(t, x)$, velocity $v(t, x)$ and pressure $p(t, x)$ distributions along the axial dimension x of the tube. The one-dimensional model is a reasonable approximation to the true three-dimensional physics since the Rike tube has a high aspect ratio, and therefore the important fluctuations of ρ, v and p are primarily in the axial direction. The equations are

$$\begin{bmatrix} \frac{\partial \rho}{\partial t} \\ \frac{\partial v}{\partial t} \\ \frac{\partial p}{\partial t} \end{bmatrix} = - \begin{bmatrix} v & \rho & 0 \\ 0 & v & \frac{1}{\rho} \\ 0 & \gamma p & v \end{bmatrix} \begin{bmatrix} \frac{\partial \rho}{\partial x} \\ \frac{\partial v}{\partial x} \\ \frac{\partial p}{\partial x} \end{bmatrix} + \begin{bmatrix} 0 \\ 0 \\ \overline{\gamma} q \end{bmatrix}, \qquad (5)$$

where $q(t, x)$ denotes the external heat power added per unit volume, and acts as an input (source term). The nonlinear equations are written in a matrix-vector form which is convenient later for linearization. Depending on the steady conditions about which these equations are linearized, the resulting linearization is a one-dimensional linear PDE that looks like a wave equation, and thus describes acoustic wave propagation. The linearization of the above equations will form the "tube acoustics" block in Figures 14 and 15.

Actuation and Sensing

The Rijke tube has both ends open, which is typically modeled by having pressure boundary conditions held at the ambient atmospheric pressure. The bottom end however is very close to the actuating speaker, and while a true model of the influence of the speaker involves accounting for inward radiating waves, a simple and reasonable approximation is to assume the speaker signal as pressure fluctuations at the bottom end. Thus the pressure boundary conditions for the system (5) are

$$\begin{aligned} p(t, 0) &= p_0 + u(t), \\ p(t, L) &= p_0, \end{aligned} \qquad (6)$$

where p_0 is the ambient pressure, and $u(t)$ is the speaker signal. Note that $u(t)$ acts as an input to the gas dynamics, but it is not distributed. The same holds for the measurement through a microphone, which is a pressure sensor whose output is (proportional to) the pressure $p(t, x_m)$ at the microphone

Sidebar 2: One-dimensional Compressible Gas Dynamics

Acoustic phenomena occur in compressible fluids. In full generality, the dynamics of such fluids are often modeled by the Euler equations of gas dynamics. Since the Rijke tube has a large aspect ratio, the geometry is simplified so that all variations of pressure, density and velocity can be assumed to occur only along the axial direction. Therefore a simpler one-dimensional mathematical model of compressible gas dynamics is sufficient to describe thermoacoustic phenomena in the Rijke tube. The three physical laws of (1) Conservation of mass, (2) Momentum balance, and (3) Energy balance can be used to derive three PDEs for one-dimensional gas dynamics as shown here.
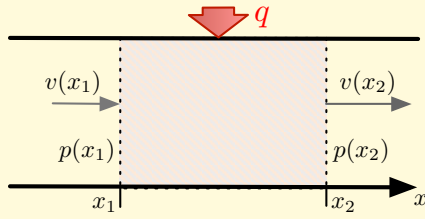

Figure 17. A small "control volume" used to account for density, momentum and energy balances in a 1-D model. The time rate of change of a quantity inside the volume $[x_1, x_2]$ is equal to the flux through the boundaries x_1 and x_2 of quantities that influence it.

To begin with, consider a one-dimensional medium with a control volume between x_1 and x_2 as illustrated in Figure 17. Let $\psi(t, x)$ and $\phi(t, x)$ be two spatially distributed fields that satisfy a flux-type relationship

$$\frac{d}{dt}\left(\int_{x_1}^{x_2} \psi(t, x)\, dx\right) = \phi(t, x)\Big|_{x_1}^{x_2},$$

which states that the time rate of change of the total quantity of ψ in $[x_1, x_2]$ is given by the value of ϕ at the boundaries x_1 and x_2. Dividing the above equation by $(x_2 - x_1)$ and taking the "small-volume limit" of $(x_2 - x_1) \to 0$ results in the PDE

$$\frac{\partial \psi}{\partial t}(t, x) = \frac{\partial \phi}{\partial x}(t, x).$$

This accounting procedure can now be performed for the gas' density $\rho(t, x)$, momentum $\rho(t, x)v(t, x)$, and internal energy $\rho(t, x)U(t, x)$ distributions. For a "calorically perfect" gas that also satisfies the ideal gas law, the internal energy (which accounts for the energy stored in molecular motion and vibration) can be expressed in terms of the pressure field by $U(t, x) = \frac{c_v}{R}p(t, x)$, where c_v and R are the specific heat capacity and universal gas constant respectively. The derivation of the three physical laws is outlined in Table I in a simplified setting that neglects effects such as heat conduction within the gas, its viscosity, and external forces. These effects can be easily added to that derivation as needed.

An exercise in algebra and the product rule of differentiation allows one to rewrite the PDEs of Table I in the following more standard form

$$\frac{\partial}{\partial t}\begin{bmatrix} \rho \\ v \\ p \end{bmatrix} = -\begin{bmatrix} v & \rho & 0 \\ 0 & v & \frac{1}{\rho} \\ 0 & \gamma p & v \end{bmatrix}\begin{bmatrix} \frac{\partial \rho}{\partial x} \\ \frac{\partial v}{\partial x} \\ \frac{\partial p}{\partial x} \end{bmatrix} + \begin{bmatrix} 0 \\ 0 \\ \bar{\gamma}q \end{bmatrix},$$

where $\gamma := 1 + \frac{R}{c_v}$ is the heat capacity ratio of the gas ($\gamma = 1.4$ for diatomic gases like air), $\bar{\gamma} := \gamma - 1$, and $q(t, x)$ denotes the heat power added per unit volume. These equations are the one-dimensional version of the Euler equations of gas dynamics; the matrix-vector form they are written in is particularly convenient for linearization.

Balance in Control Volume	PDE
Mass Conservation $\frac{d}{dt} \int_{x_1}^{x_2} \rho\, dx = \rho v \big|_{x_1}^{x_2}$ $\underbrace{\qquad}_{\substack{\text{total mass} \\ \text{in control volume}}} \underbrace{\qquad}_{\substack{\text{mass influx} \\ \text{through boundaries}}}$	$\frac{\partial}{\partial t}\rho = \frac{\partial}{\partial x}(\rho v)$
Momentum Balance $\frac{d}{dt} \int_{x_1}^{x_2} \rho v\, dx = v(\rho v)\big|_{x_1}^{x_2} + p\big|_{x_1}^{x_2}$ $\underbrace{\qquad}_{\substack{\text{total momentum} \\ \text{in control volume}}} \underbrace{\qquad}_{\substack{\text{momentum influx} \\ \text{through boundaries}}} \underbrace{\qquad}_{\substack{\text{total force} \\ \text{at boundaries}}}$	$\frac{\partial}{\partial t}(\rho v) = \frac{\partial}{\partial x}(\rho v^2 + p)$
Energy Balance $\frac{d}{dt} \int_{x_1}^{x_2} \left(\rho U + \frac{\rho v^2}{2}\right) dx = v\left(\rho U + \frac{\rho v^2}{2}\right)\Big|_{x_1}^{x_2} + pv\big|_{x_1}^{x_2} + \int_{x_1}^{x_2} q\, dx$ $\underbrace{\qquad}_{\substack{\text{total energy} \\ \text{in control volume}}} \underbrace{\qquad}_{\substack{\text{power added by} \\ \text{material influx}}} \underbrace{\qquad}_{\substack{\text{work rate of} \\ \text{pressure forces}}} \underbrace{\qquad}_{\substack{\text{heat power} \\ \text{added}}}$	$\frac{\partial}{\partial t}\left(\rho U + \frac{\rho v^2}{2}\right) = \frac{\partial}{\partial x}\left(v\left(\rho U + \frac{\rho v^2}{2}\right) + pv\right) + q$

TABLE I
DERIVATION OF THE BASIC PDEs OF ONE-DIMENSIONAL GAS DYNAMICS.

Sidebar 3: Boundary Layer Effect on Heat Release

When heat is transferred from a hot surface to a gas in steady relative motion, the heat transfer coefficient's dependence on gas velocity is captured by King's law

$$\text{heat transfer coefficient} \quad \sim \quad \kappa + \kappa_v \sqrt{|v|}. \quad \text{(S1)}$$

When gas velocity is not constant but fluctuating, this dependence has dynamics as well. Lighthill [18] analyzed these dynamics in great detail — incidentally, the author was inspired to this investigation by the Rijke tube.
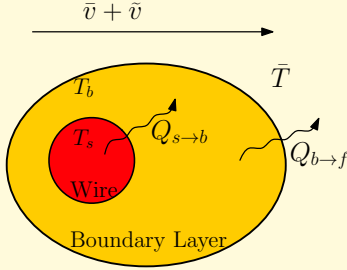

Figure S6.   Illustration of the boundary layer's effect on coil-to-gas heat transfer. Intuitively, the boundary layer depicted by the orange ellipse can be imagined as a blob of stagnant air. Heat transfer from the boundary layer into the free stream, denoted by $Q_{b \to f}$, reacts instantly to changes in the free stream velocity $\bar{v} + \widetilde{v}$ according to King's law (S1), but heat $Q_{s \to b}$ transferred from the wire needs to propagate through the boundary layer before reaching the free stream, leading to a first-order lag from flow velocity $\widetilde{v}$ to heat release $\widetilde{q}$ fluctuations.

Whenever flowing fluid comes into contact with a solid, a boundary layer is formed, and it is found that the thermal inertia of the boundary layer around the wire can be modeled by a simple first order lag, i.e. a transfer function

of the form $1/(t_{\text{hr}}s + 1)$. An estimate for the corresponding time constant is given by [18]

$$t_{\text{hr}} = 0.2 \frac{d_{\text{wire}}}{\bar{v}} = \frac{\text{diameter of the wire}}{5 \cdot \text{steady free stream velocity}}.$$

Cascading the static and dynamic dependence of the heat transfer on the velocity leads to the model (9).

As has been observed in [18] already, this lag, even if it is very small, is crucial for the model to be valid. In the current setting, this can be demonstrated nicely by considering the root locus for the model without lag (corresponding to $t_{\text{hr}} \equiv 0$), shown in Figure S7. This root locus predicts a humming frequency of roughly 282Hz, which is twice what is observed in experiments.
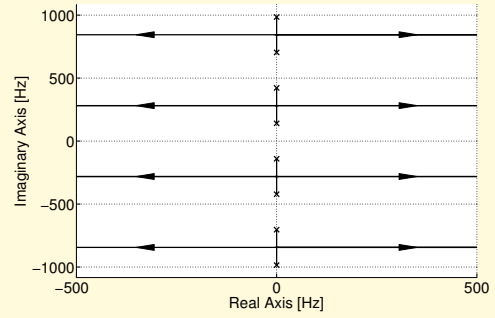

Figure S7.   What the root locus of Figure 16 would look like if the wire's thermal boundary layer effect was ignored. This amounts to assuming $t_{\text{hr}} = 0$, or equivalently ignoring the first order lag in the heat release response. The fundamental frequency branch which moves into the right half plane is now incorrectly predicted to be twice what is observed in experiments. This illustrates that including the first-order lag is crucial to correctly predict thermoacoustic instabilities.

---

location x_m. The controller used to stabilize the tube connects those two signals via a proportional control feedback loop.

Heat Transfer

The Euler equations (5) have an external heat input $q(t,x)$ as a source term, which can be used to model heat released from the coil into the gas. If the coil is assumed to be located in a very narrow section at location x_o, then a reasonable approximation to this distributed input is

$$q(t,x) = \frac{1}{A} \, \delta(x - x_o) \, Q(t), \quad \text{(7)}$$

where δ is the Dirac impulse with units 1/m, $Q(t)$ is the heat power released from the coil in W, and A is the tube cross section.

The next key step is to quantify the dependence of coil-to-gas heat power released $Q(t)$ on the flow velocity $v(x_o,t)$ near the wire. Heat is transferred from a solid to a gas due to both conduction and convection. Convection depends on

the velocity v of the gas, whereas conduction does not; both depend on the temperature difference. King's law [17] is a commonly used approximation for these dependencies, and in the current context it states that in steady flow, the heat power transfer Q_K of a hot circular wire of length l_w in a colder fluid flow is

$$Q_K = l_w \left(\kappa + \kappa_v \sqrt{|v|} \right) (T_{\text{wire}} - T_{\text{gas}}), \quad \text{(8)}$$

where κ is the fluid's thermal conductivity, and κ_v is a constant that is largely empirically determined. The first term is Fourier's law of heat conduction, while the second term expresses that convective heat transfer occurs at a rate proportional to $\sqrt{|v|}$. The formula suggests that heat transfer is enhanced by flow velocity, regardless of direction, but the "rate of enhancement" tapers off as velocity increases.

King's law does not include any temporal dynamics. However, if the gas velocity fluctuates, there are important dynamic effects to be considered, and it will turn out that their inclusion is crucial to correctly predicting the frequency of the hum. These dynamics are mainly due to a boundary layer

forming around the wire, which has its own thermal inertia. Figure S6 and "Boundary Layer Effect on Heat release" explain this effect. An intuitive picture is to imagine this boundary layer as a blob of stagnant air, through which the heat needs to be conducted before reaching the free stream of gas outside the boundary layer. The conclusion is that this boundary layer effect introduces a first-order lag into the heat release process which now can be modeled by

$$t_{\mathrm{hr}}\dot{Q}(t) = -Q(t) + Q_K(t) \tag{9a}$$

$$Q_K(t) = l_w(T_{\mathrm{wire}} - T_{\mathrm{gas}}) \left(\kappa + \kappa_v \sqrt{|v(t,x_0)|} \right). \tag{9b}$$

Note how the mapping from $v(\cdot, x_o)$ to Q_K in (9b) is the memoryless nonlinearity in the bottom loop of Figure 15, while Equation (9a) represents the first order lag.

The above model tacitly assumed that T_{gas} is constant, but in reality it fluctuates together with pressure and density. It is shown in a subsequent section (see Figure 18) that this effect is much less significant than the dependence on velocity fluctuations, and therefore the diagram of Figure 15 has only the velocity fluctuations as an input to the heat release mechanism.

Linearization of the Acoustics

The full system is described by **(a)** the gas dynamics (5), the boundary conditions (6) and heat input (7), which are in feedback with **(b)** the heat release model consisting of King's law (9b) and the first-order lag (9a) of the boundary layer effect. The two subsystems of gas dynamics and heat release can be linearized separately. The linearization of the former yields linear acoustic dynamics, and while the linearization of the latter is straightforward, an analysis of the involved parameters reveals that velocity fluctuations are significantly more important than pressure and density fluctuations in the feedback path.

Linearization of the nonlinear model (5) requires knowing the steady state conditions. An accurate calculation of the steady state requires incorporating buoyancy effects (to model steady upward flow due to steady heat release from the coil) as well as the steady temperature and density variations along the tube length (e.g. gas in the upper section is hotter than that in lower section). However since the important parameter in acoustic dynamics is the speed of sound, and the above variations have relatively minor effect on the speed of sound, an alternative and much simpler equilibrium can be used for the acoustic linearization. This simple equilibrium assumes spatially constant density, velocity, and pressure fields, which trivially satisfy the nonlinear PDEs, if there is no heat input ($q \equiv 0$) and no speaker actuation ($u \equiv 0$). Denoting a steady state by a bar $\overline{\bullet}$ and small deviations from it by a tilde $\widetilde{\bullet}$, a linearization is obtained by plugging $\rho(t,x) = \overline{\rho} + \widetilde{\rho}(t,x)$ and so on into the nonlinear equations and discarding all terms of second or higher order in the deviation variables. Applying

this process to (5) leads to

$$\frac{\partial}{\partial t} \begin{bmatrix} \widetilde{\rho} \\ \widetilde{v} \\ \widetilde{p} \end{bmatrix} = - \begin{bmatrix} \overline{v} & \overline{\rho} & 0 \\ 0 & \overline{v} & 1/\overline{\rho} \\ 0 & \gamma\overline{p} & \overline{v} \end{bmatrix} \frac{\partial}{\partial x} \begin{bmatrix} \widetilde{\rho} \\ \widetilde{v} \\ \widetilde{p} \end{bmatrix} + \begin{bmatrix} 0 \\ 0 \\ \overline{\gamma} \end{bmatrix} \widetilde{q}, \tag{10}$$

which very closely resembles (5) with the important difference that the "A-matrix" is now a constant matrix and hence, (10) is a linear, but infinite-dimensional state-space description of the gas dynamics with the state $\begin{bmatrix} \widetilde{\rho} & \widetilde{v} & \widetilde{p} \end{bmatrix}^T$. Furthermore, from (6) it follows immediately that $\overline{p} = p_0$, and that $\widetilde{p}(t,0) = u(t)$ and $\widetilde{p}(t,L) = 0$.

A further simplification is due to the upward flow $\overline{v}$ being very small (relative to the speed of sound); rewriting the model in dimensionless quantities shows that if $\overline{v} \ll c$, where $c = \sqrt{\gamma\overline{p}/\overline{\rho}}$ is the velocity of sound in steady state, then $\overline{v}$ can be neglected. For details see "Dimensionless Quantities" on Page 18. Setting $\overline{v}$ to zero leads to the dynamics of (10) being decoupled: The density $\widetilde{\rho}$ does not couple into the pressure/velocity dynamics and can be dropped from consideration. Therefore, the linearization of the gas dynamics yields the following wave equation with the heat fluctuations $\widetilde{Q}$ as a source term at $x = x_o$

$$\frac{\partial}{\partial t} \begin{bmatrix} \widetilde{v} \\ \widetilde{p} \end{bmatrix} = \begin{bmatrix} 0 & -\frac{1}{\overline{\rho}} \\ -\gamma\overline{p} & 0 \end{bmatrix} \frac{\partial}{\partial x} \begin{bmatrix} \widetilde{v} \\ \widetilde{p} \end{bmatrix} + \begin{bmatrix} 0 \\ \frac{\overline{\gamma}}{A} \end{bmatrix} \delta(x - x_o) \, \widetilde{Q}(t). \tag{11}$$

The boundary conditions on pressure and the speaker signal u can be written in the general form

$$\begin{bmatrix} 1 \\ 0 \end{bmatrix} u(t) = \begin{bmatrix} 0 & 1 \\ 0 & 0 \end{bmatrix} \begin{bmatrix} \widetilde{v}(t,0) \\ \widetilde{p}(t,0) \end{bmatrix} + \begin{bmatrix} 0 & 0 \\ 0 & 1 \end{bmatrix} \begin{bmatrix} \widetilde{v}(t,L) \\ \widetilde{p}(t,L) \end{bmatrix}. \tag{12}$$

The two equations (11) and (12) represent the LTI dynamics of acoustics driven by the two scalar inputs $\widetilde{Q}(t)$ and $u(t)$. The remaining task is to find an expression for the transfer functions from those two inputs to the pressure and velocity at any location within the tube as outputs. A standard technique is to apply the Laplace transform to (11) and (12), and rearrange so that the spatial derivative is on the left hand side of the equation. Then, one obtains an ordinary differential equation with boundary conditions

$$\begin{bmatrix} \mathcal{V}'(s,x) \\ \mathcal{P}'(s,x) \end{bmatrix} = \begin{bmatrix} 0 & \frac{-s}{\gamma\overline{p}} \\ -s\overline{\rho} & 0 \end{bmatrix} \begin{bmatrix} \mathcal{V}(s,x) \\ \mathcal{P}(s,x) \end{bmatrix} + \begin{bmatrix} \frac{\overline{\gamma}/\gamma}{\overline{p}A} \\ 0 \end{bmatrix} \delta(x-x_o)\widetilde{\mathcal{Q}}(s)$$

$$\begin{bmatrix} 1 \\ 0 \end{bmatrix} \mathcal{U}(s) = \begin{bmatrix} 0 & 1 \\ 0 & 0 \end{bmatrix} \begin{bmatrix} \mathcal{P}(s,0) \\ \mathcal{P}(s,0) \end{bmatrix} + \begin{bmatrix} 0 & 0 \\ 0 & 1 \end{bmatrix} \begin{bmatrix} \mathcal{P}(s,L) \\ \mathcal{P}(s,L) \end{bmatrix}, \tag{13}$$

where $\mathcal{V}(s,x), \mathcal{P}(s,x), \mathcal{U}(s)$ and $\mathcal{Q}(s)$ are the Laplace transforms (in t) of $\widetilde{v}(t,x)$, $\widetilde{p}(t,x)$, $u(t)$ and $\widetilde{q}(t)$ respectively, and differentiation in x is denoted by prime, e.g. $\mathcal{V}'(s,x) := \frac{d}{dx}\mathcal{V}(s,x)$. The Laplace transform variable s can be simply regarded as a parameter in the above differential equation which can now be treated as an ODE (in x) with two point boundary conditions. A general formula (S10) for the solution of this TPBVP is derived in "Transfer Function Computation for Two-Point Boundary Value Problems." Application of this procedure to (13) yields the transfer function matrix (3).

Linearization of the Heat Release

To facilitate interconnection of heat release and acoustic models, the temperature T in King's law (9b) can be expressed in terms of the state variables of acoustics p and ρ by using the ideal gas law $T = p/(\rho R)$ — note that now, T_{gas} is not initially assumed to be constant, but it is shown in "Dimensionless Quantities" on Page 18 that its contribution (expressed with pressure and density) can be neglected. As in the preceding section, all variables are then expressed as steady state plus deviation, e.g. $v = \bar{v} + \tilde{v}$, and the linearized version of (9b) takes the three-input form

$$\widetilde{Q}_K = \begin{bmatrix} f(\bar{v})\frac{\overline{T}}{\bar{\rho}} & f'(\bar{v})\left(T_{\mathrm{wire}} - \overline{T}\right) & -f(\bar{v})\frac{\overline{T}}{\bar{p}} \end{bmatrix}\begin{bmatrix} \widetilde{\rho} \\ \widetilde{v} \\ \widetilde{p} \end{bmatrix}, \quad \text{(14)}$$

conveniently written as a vector gain multiplying the acoustic states. $\overline{T} = \bar{p}/(\bar{\rho}R)$ is the steady-state temperature and simply a parameter, and $f(v) = l_w(\kappa + \kappa_v\sqrt{|v|})$ is the velocity-dependent heat transfer coefficient according to King's law (8).

This representation of the heat release dynamics illustrates nicely that while all three state variables influence the heat transfer process, they do so with different gains, and so it is no surprise that this model can also be simplified substantially by considering the relative sizes of those gains: careful dimensional analysis of the linearization shows velocity fluctuations to be the main driver of heat release dynamics when the flow is very subsonic (i.e. $\bar{v} \ll c$), for details see Sidebar "Dimensionless Quantities" on Page 18. It is thus reasonable to proceed with the single-input linearized version of (9b)

$$\widetilde{Q}_K = f'(\bar{v})\left(T_s - \overline{T}\right)\widetilde{v}.$$

Symbol		Value Used
$\overline{\rho}$	Density	1.2 kg/m^3
$\overline{p}$	Pressure	10^5 N/m^2
$c = \sqrt{\gamma \frac{\overline{p}}{\overline{\rho}}}$	Speed of Sound	343 m/s
c_p, c_v	Heat Capacities	1008, 718 J/(kg K)
$\gamma = c_p/c_v$	Adiabatic Ratio	1.4
$R = c_p - c_v$	Ideal Gas Constant	290 J/(kg K)
L	Tube Length	1.219 m
t_{hr}	Heat Release Time Constant	$\approx 3.5 \; 10^{-4}$ s

TABLE II
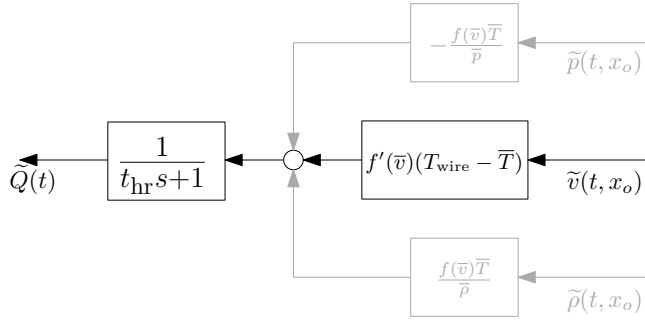
VALUES OF RELEVANT PARAMETERS USED FOR COMPUTATIONS.

Figure 18. A signal flow diagram of the linearized heat release model. The analysis in "Dimensionless Quantities" shows that the gains of the local acoustic pressure $\widetilde{p}(t, x_o)$ and the local density variation $\widetilde{\rho}(t, x_o)$ are much smaller than the gain of the local acoustic velocity $\widetilde{v}(t, x_o)$, hence they may be neglected.

Figure 18 depicts this reduction graphically. For the range of steady velocities $\bar{v}$ in the Rijke tube experiment, the nonlinear heat release dynamics (bottom loop of Figure 15) are hence only a function of velocity fluctuations and the linearization is represented compactly by the transfer function

$$B(s) = \frac{f'(\overline{v})(T_s - \overline{T})}{t_{\mathrm{hr}} s + 1} \tag{15}$$

between local velocity fluctuations $\widetilde{v}(t, x_o)$ and heat released into the gas $\widetilde{Q}(t)$, see also Figures 15 and 18.

It should be stressed here that the significance of the steady buoyancy-induced upward velocity $\overline{v}$ is very different for the heat release than for the gas dynamics. The wave-like equation (11) for the gas dynamics was obtained by assuming $\overline{v} \approx 0$ with the justification that the dynamics would not change much if $\overline{v}$ were nonzero but small. For the heat transfer, however, assuming no steady upward component in the velocity would result in an invalid linearization, since the derivative of $\sqrt{|\cdot|}$ is discontinuous at 0. The importance of the offset in velocity lies in moving to the "linearizable part" of the square root function, as depicted in the bottom block in Figure 15.
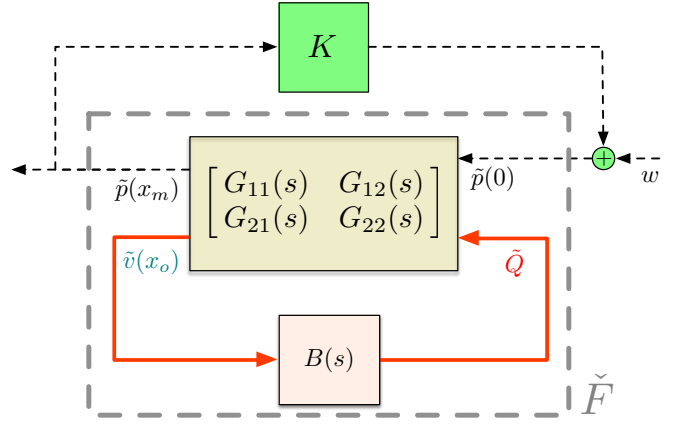

Figure 19. The modeled transfer function between speaker input and microphone output signals can be represented – with linearized heat release – as a lower linear fractional transformation $\check{F} = G_{11} + G_{12}BG_{21}/(1 - G_{22}B)$.

Comparison of Modeling and Empirical Results

Finally, the previous modeling efforts can be used to test how closely the physical model (3) corresponds to reality (or rather the identified model as a proxy for reality) beyond explaining the thermoacoustic oscillations. It is important to understand first the relationship between the modeled and identified transfer functions. The open-loop Bode plot of Figure 8 corresponds to the identified response $F(e^{j\omega})$ of pressure fluctuations as measured by the microphone to pressure fluctuations induced by the speaker; in the model depicted in Figure 15, this is the transfer function from $\widetilde{p}(0)$ to $\widetilde{p}(x_m)$ (with w and K set to zero), including the (linearized) heat release feedback loop; for clarity, this is illustrated in Figure 19.

Comparisons need to be made between the identified open loop $F(e^{j\omega})$ and

$$\check{F}(s) = G_{11}(s) + \frac{G_{12}(s)B(s)G_{21}(s)}{1 - G_{22}(s)B(s)}.$$

There remain however several unknown parameters in the model: an overall gain due to the unknown conversion factors of speaker and microphone, the microphone position x_m, and linear gain and time constant t_{hr} of the heat release feedback $B(s)$. Additionally, the assumptions about friction, diffusive effects, and the steady upward flow that were made during the modeling of the gas dynamics — and had the advantage that the very simple model (11) and transfer function (3) could be obtained — also lead to system poles moving onto the imaginary axis, which made necessary the less-than-rigorous argument that intuitively, the neglected damping would move the poles towards the left (rendering them stable), and presents a clinical case which makes comparisons difficult. "Wave Dynamics with Diffusion and Damping" addresses the issue numerically and Figure S13 suggests that the poles lie on a parabola shape.
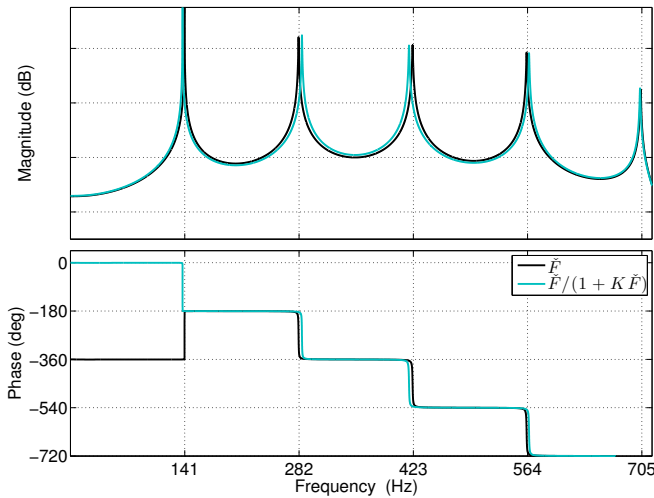
Figure 20. Bode plots of open-loop ($K = 0$) and closed-loop (with a stabilizing $K \neq 0$) frequency responses derived from the physical model of Figures 19 and 15. Note the opposite signs of the 180° phase increase near the fundamental mode indicating open-loop instability and closed-loop stability of that mode.

If the damping effect is imitated by considering $j\omega + \varepsilon_0 + \varepsilon_1\omega^2$ instead of $j\omega$, and choices of the unknown heat release time constant, heat release gain and feedback gain are made judiciously, one obtains the responses shown in Figure 20; remarkably, despite employing very simple devices to treat the aforementioned difficulties, these responses qualitatively capture the most important features of Figures 7 and 8: resonant peaks, a phase increase of 180° at the first peak for the unstabilized open loop $\check{F}$, and phase drops of the same amount at the higher-order peaks for $\check{F}$ and at all peaks for the stabilized closed loop $\check{F}/(1 + K\check{F})$. That it is easy to find a wide range of parameter values that generate responses with these features after only a few manual iterations can be seen as evidence that the physical model indeed captures the important structures of the underlying physics.

Summary

The Rijke tube experiment has been presented from a control engineer's perspective. To emphasize this perspective, the first part of the paper showed how one can approach this experiment using "black box" techniques such as system identification and model validation. Although a great deal of insight can be obtained from these generic systems techniques, a thorough understanding of the underlying dynamics is achieved by physical modeling from first principles in the second part of the paper. As is typical in any control-oriented modeling exercise, choices must be made as to the right level of "granularity" of various pieces of the model. In this paper, these choices were guided by the findings in the empirical part of the investigation. A notable example is modeling the boundary layer effect on heat release from the coil, without

which the root locus arguments presented would fail to explain the observed limit cycle frequencies in the experiment. While a full fidelity model of that boundary layer would be rather complex, it was shown that a first-order lag model for that boundary layer is sufficient to produce consistent predictions. This back and forth cross validation between modeling and experiment can serve as an instructive pedagogical device.

Thermoacoustic effects are mostly known within the controls community as undesirable phenomena that need to be regulated [2], [19], [3], [20], [21], [6], [22]. There is however another perspective in which these effects can be regarded as an *energy conversion* mechanism. In the Rijke tube, the thermoacoustic instability produces a limit cycle which can be thought of as a mechanism of converting some of the steady heater power into acoustic power radiated from the tube. This is only one example of several types of thermoacoustic engines in which powerful, internally contained acoustic waves perform the mechanical work in the energy conversion process [23], [24]. Thus acoustic waves replace the traditional pistons, cranks and turbines typical in traditional heat engines, and can therefore potentially have very high efficiencies. With some notable exceptions [25], [26], [27], these devices have not received much attention from control engineers. Although the Rijke tube is not a useful heat engine, the underlying energy conversion mechanisms are sufficiently similar to thermoacoustic engines to render it a simple and useful experimental testbed for active control of thermoacoustic phenomena.

References

[1] P. Rijke, "Über eine neue Art, die in einer an beiden Enden offenen Röhre enthaltene Luft in Schwingungen zu versetzen," *Annalen der Physik*, vol. 183, pp. 339–343, 1859.

[2] J. Hathout, A. Annaswamy, M. Fleifil, and A. Ghoniem, "A model-based active control design for thermoacoustic instability," *Combustion Science and Technology*, vol. 132, no. 1, pp. 99–138, 1998.

[3] A. Annaswamy, M. Fleifil, J. Rumsey, R. Prasanth, J. Hathout, and A. Ghoniem, "Thermoacoustic instability: model-based optimal control designs and experimental validation," *IEEE Transactions on Control Systems Technology*, vol. 8, no. 6, pp. 905–918, 2000.

[4] A. McIntosh, "Flame resonance and acoustics in the presence of heat loss," *Lectures in Applied Maths*, vol. 24, no. Part 1, pp. 269–301, 1986.

[5] A. McIntosh, "On flame resonance in tubes," *Combustion Science and Technology*, vol. 69, no. 4-6, pp. 147–152, 1990.

[6] A. P. Dowling and A. S. Morgans, "Feedback control of combustion oscillations," *Annu. Rev. Fluid Mech.*, vol. 37, pp. 151–182, 2005.

[7] M. Juniper, "Triggering in the horizontal Rijke tube: non-normality, transient growth and bypass transition,"

Sidebar 5: Dimensionless Quantities

It is common practice in fields such as fluid dynamics or heat transfer to express physical relationships in terms of dimensionless quantities, and for good reasons: it often leads to a reduced number of parameters, allows to compare relative sizes more easily, and last but not least leads to aesthetically more appealing equations.

In the model equations for the Rijke tube, there are three dependent variables, namely ρ, v, and p, and the two independent variables x and t. Variables are non-dimensionalized by setting them in relation to some reference value; a natural reference value for the pressure p would be its nominal value, the atmospheric pressure $p_0 = \overline{p}$, similarly for ρ. The situation is different for the velocity v: it is expected that the nominal velocity $\overline{v}$ is very small, hence scaling v by $\overline{v}$ would lead to a large quantity, not comparable to the scaled pressure and density. In other words: While the percentage change in p and ρ will be small, the percentage change in v will be large. Thus, the velocity is scaled by c, the speed of sound, and the set of scaled variables is

$$\psi := p/\overline{p}, \qquad m := v/c, \text{ and } \qquad r := \rho/\overline{\rho}.$$

Similarly, scaling the spatial variable x by the tube length L and time t by the time it takes sound to propagate through the entire tube yields

$$\xi := x/L, \qquad \tau := ct/L,$$

and

$$\frac{\partial}{\partial \xi} = L\frac{\partial}{\partial x}, \qquad \frac{\partial}{\partial \tau} = \frac{L}{c}\frac{\partial}{\partial t}.$$

Rewriting, for example, the conservation of momentum equation (see Table I) using dimensionless variables and the relation $c^2 = \gamma\overline{p}/\overline{\rho}$ leads to

$$\frac{\partial m}{\partial \tau} = -m\frac{\partial m}{\partial \xi} - \frac{1}{\gamma r}\frac{\partial \psi}{\partial \xi}.$$

Rewriting the state-space model (10) in terms of the dimensionless variables, yields the more appealing dimensionless form

$$\frac{\partial}{\partial \tau}\begin{bmatrix} \widetilde{r} \\ \widetilde{m} \\ \widetilde{\psi} \end{bmatrix} = -\begin{bmatrix} \text{Ma} & 1 & 0 \\ 0 & \text{Ma} & \frac{1}{\gamma} \\ 0 & \gamma & \text{Ma} \end{bmatrix}\frac{\partial}{\partial \xi}\begin{bmatrix} \widetilde{r} \\ \widetilde{m} \\ \widetilde{\psi} \end{bmatrix} + \begin{bmatrix} 0 \\ 0 \\ \mathring{q} \end{bmatrix}, \quad \text{(S19)}$$

where $\widetilde{\bullet}$ again signifies deviation from steady state, $\text{Ma} := \overline{v}/c$ is the famous Mach number, and $\mathring{q} := \frac{\bar{\gamma}L}{\overline{p}c}q$ simply lumps q with several parameters to obtain a dimensionless input.

Using (S19), the case for neglecting the diagonal elements in (10) can now be made more rigorous: without computation or measurement, it is clear that $\text{Ma} \ll 1$, whereas γ is of order unity, hence compared to γ, $\text{Ma} \approx 0$.

Similarly, rewriting (14) using the dimensionless variables, one obtains

$$\widetilde{Q}_K = \begin{bmatrix} f(\overline{v})\overline{T} & cf'(\overline{v})(T_{\text{wire}} - \overline{T}) & -f(\overline{v})\overline{T} \end{bmatrix}\begin{bmatrix} \widetilde{r} \\ \widetilde{m} \\ \widetilde{\psi} \end{bmatrix}.$$

Comparison of the gains of $\widetilde{r}$ and $\widetilde{\psi}$ on the one hand, and $\widetilde{m}$ on the other leads to

$$\frac{f(\overline{v})}{cf'(\overline{v})(T_{\text{wire}} - \overline{T})} = 2\frac{\overline{T}}{T_{\text{wire}} - \overline{T}}\left(\frac{\kappa}{\kappa_v\sqrt{\overline{v}}} + 1\right)\text{Ma}.$$

If all terms except for Ma can be expected to be of order unity or less, then it is justified to neglect the contributions of density and pressure variations to the heat transfer. The only term in question is $\kappa/(\kappa_v\sqrt{\overline{v}})$, the ratio between conductive and convective heat transfer; these are typically comparable – see [17, Tables V & VI, note that velocities are measured in cm/s] – and hence this term is of order unity, too.

J. Fluid Mech, vol. 667, pp. 272–308, 2011.

[8] M. Heckl and M. Howe, "Stability analysis of the Rijke tube with a Green's function approach," *Journal of Sound and Vibration*, vol. 305, pp. 672–688, 2007.

[9] I. Gustavsson, L. Ljung, and T. Söderström, "Identification of processes in closed loop—identifiability and accuracy aspects," *Automatica*, vol. 13, no. 1, pp. 59 – 75, 1977.

[10] U. Forssell and L. Ljung, "Closed-loop identification revisited," *Automatica*, vol. 35, no. 7, pp. 1215–1241, 1999.

[11] L. Ljung, *System Identification: Theory for the User*. PTR Prentice Hall, Upper Saddle River, NJ, 1999.

[12] ——, *System Identification Toolbox for Use with MATLAB*, The MathWorks, Inc., 2007.

[13] R. De Callafon, P. M. Van den Hof *et al.*, "FREQID – frequency domain identification toolbox for use with MATLAB," *Selected Topics in Identification, Modelling and Control*, vol. 9, pp. 129–134, 1996.

[14] R. De Callafon, "http://mechatronics.ucsd.edu/freqid/."

[15] D. Bayard, "Statistical plant set estimation using Schroeder-phased multisinusoidal input design," *Applied Mathematics and Computation*, vol. 58, no. 2, pp. 169–198, 1993.

[16] J. Burgess, "Chirp design for acoustical system identification." *The Journal of the Acoustical Society of America*, vol. 91, no. 3, p. 1525, 1992.

[17] L. V. King, "On the convection of heat from small cylinders in a stream of fluid: determination of the convection constants of small platinum wires with applications to hot-wire anemometry," *Philos. Trans. Royal Soc.*, pp. 373–432, 1914.

[18] M. Lighthill, "The response of laminar skin friction and heat transfer to fluctuations in the stream velocity," *Proceedings of the Royal Society of London. Series A. Mathematical and Physical Sciences*, vol. 224, no. 1156, pp. 1–23, 1954.

[19] A. Banaszuk, K. B. Ariyur, M. Krstić, and C. A. Jacob-

Sidebar 6: Wave Dynamics with Diffusion and Damping

Adding thermal diffusion, viscosity and wall friction to the equations in the right column of Table I, linearizing and rewriting in nondimensional form as outlined in "Dimensionless Quantities," one obtains

$$\frac{\partial}{\partial \tau}\begin{bmatrix}\widetilde{r}\\ \widetilde{m}\\ \widetilde{\psi}\end{bmatrix} = \begin{bmatrix}0 & 0 & 0\\ \mathrm{Ma}\bar{\beta} & -\bar{\beta} & 0\\ 0 & 2\mathrm{Ma}\gamma\bar{\beta} & 0\end{bmatrix}\begin{bmatrix}\widetilde{r}\\ \widetilde{m}\\ \widetilde{\psi}\end{bmatrix} -$$

$$\begin{bmatrix}\mathrm{Ma} & 1 & 0\\ 0 & \mathrm{Ma} & \frac{1}{\gamma}\\ 0 & \gamma & \mathrm{Ma}\end{bmatrix}\frac{\partial}{\partial \xi}\begin{bmatrix}\widetilde{r}\\ \widetilde{m}\\ \widetilde{\psi}\end{bmatrix} +$$

$$\phi\begin{bmatrix}0 & 0 & 0\\ 0 & \mathrm{Pr}/\gamma & 0\\ -1 & 0 & 1\end{bmatrix}\frac{\partial^2}{\partial \xi^2}\begin{bmatrix}\widetilde{r}\\ \widetilde{m}\\ \widetilde{\psi}\end{bmatrix} + \begin{bmatrix}0\\ 0\\ \mathring{q}\end{bmatrix}, \quad \text{(S21)}$$

where $\mathrm{Pr} = \nu/\alpha$ is the Prandtl number, the ratio of kinematic viscosity and thermal diffusivity, ϕ is a dimensionless "diffusion strength" parameter, and $\bar{\beta}$ quantifies the amount of friction.

The complexity of the model has increased significantly: (S21) is of second order, due to diffusion, and in three states, since the density $\widetilde{r}$ is not decoupled anymore. In principle, the procedure of "Transfer Function Computation for Two-Point Boundary Value Problems" can still be applied, but the obtained transfer functions are too unwieldy to learn anything from them. However, the poles of any derived transfer function will be a subset of the spectrum of the right-hand-side operator, analogously to the situation in finite-dimensional LTI systems. Hence, instead of transfer function computations, the spectrum of the right-hand-side operator is computed numerically using Chebyshev spectral methods. For details on and more applications of such methods, refer to the excellent book [28].

Figure S13 shows the significant part of the spectrum obtained using $N = 192$ grid points, along with some of the pressure modes for a specific set of the parameters Ma, Pr, ϕ, and $\bar{\beta}$ representative of the conditions in the Rijke tube experiment. As expected, the spectrum is located very close to, but left of the imaginary axis, with modes corresponding to a standing half-wave and its harmonics; poles corresponding to higher frequencies are farther left, indicating more damping. It is important to note that in particular the parameters ϕ and $\bar{\beta}$, which are known only to within maybe an order of magnitude, appear to have very well-defined effects. Increasing the amount of diffusion ϕ will "bend" the spectrum, i.e. the parabola shape will become narrower, while increasing the amount of friction $\bar{\beta}$ will shift the entire spectrum towards the left. These numerical computations validate the claim made during the analysis of the root locus in Figure 16, namely that the poles located *on* the imaginary axis would be shifted towards the left if neglected diffusion and/or damping effects were retained.
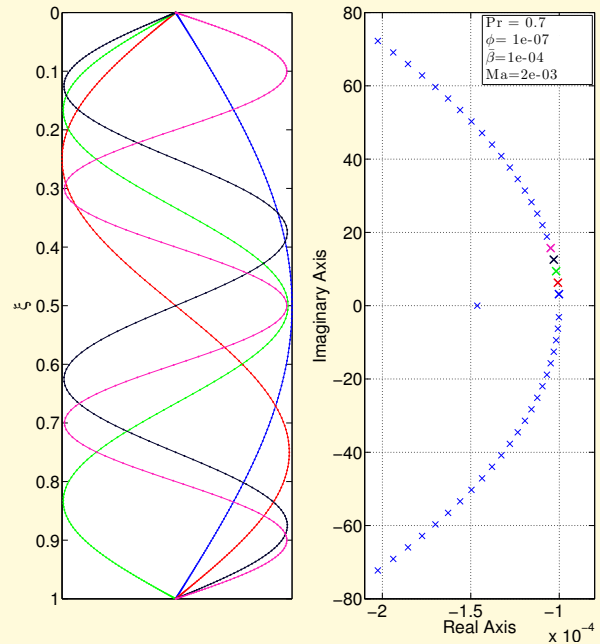

Figure S13. Numerical computation of the spectrum of the spatial differential operator in (S21). The left plot shows the five pressure modes corresponding to the fundamental and the first four harmonics; they are indistinguishable from the pressure modes of the undamped model (11), corresponding to the resonances of a tube with two open ends. The right plot shows part of the numerically computed spectrum: poles located on the imaginary axis in the case without damping are now damped, i.e. shifted to the left; higher frequencies are damped more, yet still lightly (note the axis scales).

son, "An adaptive algorithm for control of combustion instability," *Automatica*, vol. 40, no. 11, pp. 1965–1972, 2004.

[20] B. Zinn and Y. Neumeier, "An overview of active control of combustion instabilities," *35th Aerospace Sciences Meeting and Exhibit*, vol. 461, p. 1997, 1997.

[21] S. Candel, "Combustion dynamics and control: Progress and challenges," *Proceedings of the Combustion Institute*, vol. 29, no. 1, pp. 1–28, 2002.

[22] M. Heckl, "Active control of the noise from a Rijke tube,"

Journal of Sound and Vibration, vol. 124, no. 1, pp. 117–133, 1988.

[23] S. Garrett and S. Backhaus, "The power of sound," *American Scientist*, vol. 88, no. 6, p. 516, 2000.

[24] H. Madarame, "Thermally induced acoustic oscillations in a pipe. I - oscillations induced by plane heat source in air current," *JSME International Journal Series B*, vol. 24, pp. 1626–1633, 1981.

[25] Y. Li, B. L. Minner, G. T.-C. Chiu, L. Mongeau, and J. E. Braun, "Adaptive tuning of an electrodynamically driven

thermoacoustic cooler," *The Journal of the Acoustical Society of America*, vol. 111, no. 3, pp. 1251–1258, 2002.

[26] Y. Li, G. Chiu, and L. Mongeau, "Dual-driver standing wave tube: acoustic impedance matching with robust repetitive control," *Control Systems Technology, IEEE Transactions on*, vol. 12, no. 6, pp. 869–880, 2004.

[27] Y. Li, M. A. Rotea, G.-C. Chiu, L. Mongeau, and I.-S. Paek, "Extremum seeking control of a tunable thermo-acoustic cooler," *Control Systems Technology, IEEE Transactions on*, vol. 13, no. 4, pp. 527–536, July 2005.

[28] L. N. Trefethen, *Spectral Methods in MATLAB*. Society for Industrial and Applied Mathematics, 2000. [Online]. Available: http://epubs.siam.org/doi/abs/10.1137/1.9780898719598